CHAPTER 5

WEAR AND FRICTION BEHAVIOUR OF (Cu-Gr-B_4C) COMPOSITES AND CORRELATING TO THE TOPOGRAPHICAL CHARACTERISTICS

5.1 Introduction

The results of creating composites with different weight percentages of boron carbide(B_4C) and graphite (Gr) particles using the powder metallurgy method are shown in this chapter. Also displayed are the findings of the XRD analysis used to determine the phases of pure copper and its mixtures. The impact of varying weight percentages of boron carbide(B_4C) and graphite (Gr) particles on the microstructure, mechanical, and physical properties of the copper composites was investigated by various analytical techniques. The results are presented, and their ramifications are considered. The standard pin-on-disc machine has been used to study the dry sliding friction and wear behaviour of copper composites, denoted by the designations C1, C2, C3, and C4, which include pure Cu, Cu-1.5 wt.%, Gr-1.5 wt.% B_4C, Cu-3 wt.% Gr-3 wt.% B_4C, and Cu-4.5 wt.% Gr-4.5 wt.% B_4C. The normal load and sliding speed have been kept constant. For the test, a counter face made of hardened steel EN31 is utilized. The tribological properties of composite materials are significantly influenced by the reinforcements' shape, dispersion, and composition. The investigation looks at the tribological behaviours of several factors, such as sliding velocity, applied stress, sliding distance, and the weight percentage of boron carbide(B_4C). The composites' worn surfaces were inspected using an SEM connected to an EDS and an AFM. The topographical examination of deteriorated surfaces was connected to the results obtained.

5.2 Morphological study of reinforcing particles

The reinforcing phase does not always have to be in the form of long fibres. The substance can exist in various forms, such as flakes, short fibres, particles, whiskers, sheets, or continuous fibres. Hence, the present study utilises particle reinforcements to fabricate metal matrix hybrid composites. The SEM equipment is used to analyze the reinforcing particles; the results are presented in Figure 5.1. Figures 5.1 (a) to (c) depict the shapes and structures of the copper, graphite, and boron carbide(B_4C) particles, respectively. The shape of the particles typically has a significant impact on the characteristics of the material.

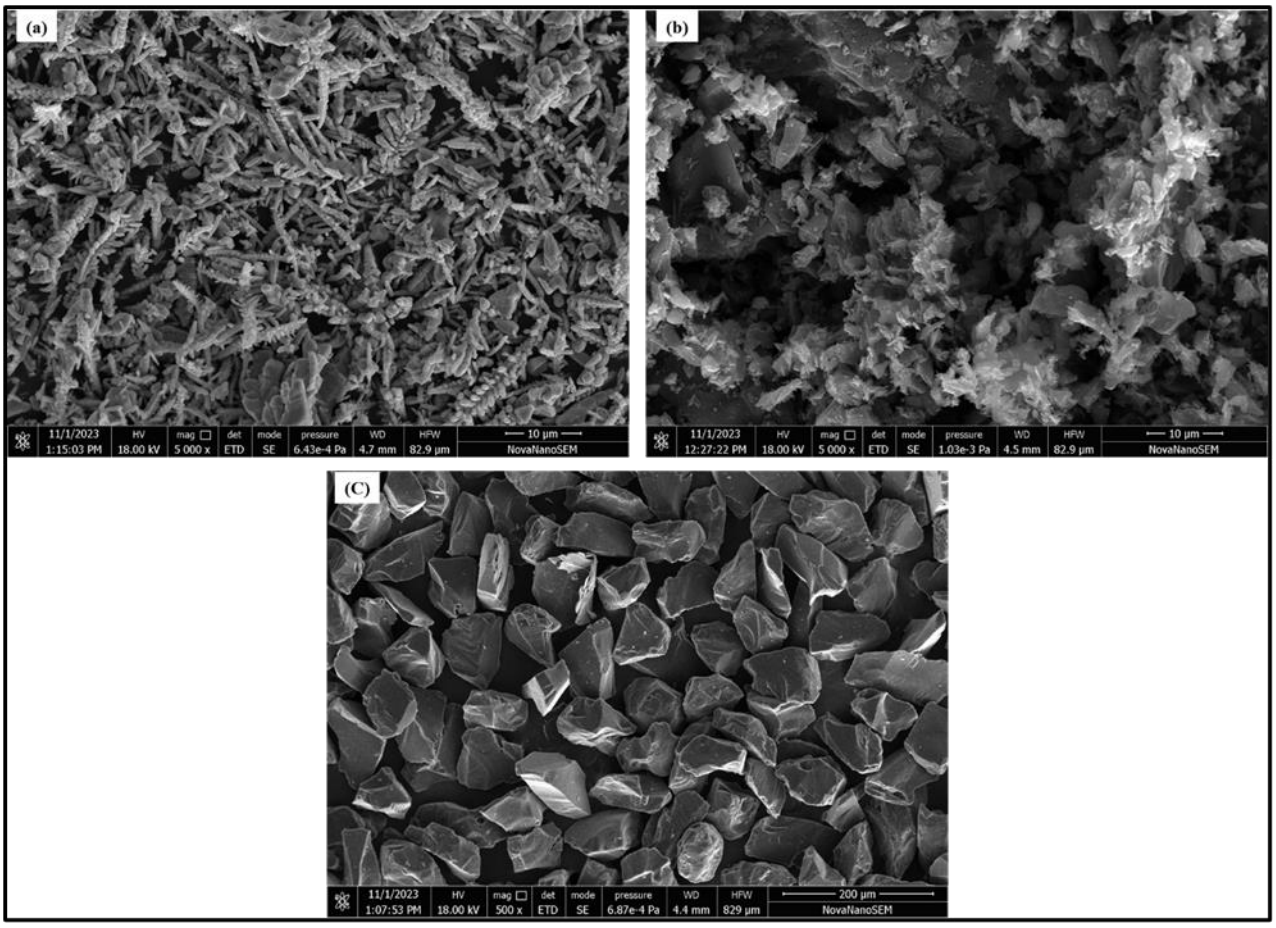

Figure 5.1. SEM micrograph of (a)pure copper powder, (b) graphite particles, and (c) boron carbide(B_4C) particles

5.3 Phase and microstructural analysis

The X-ray diffraction analysis of the sintered composite specimens in the range of 20 to 80 degrees is depicted in Figure 5.2. The most significant peaks are observed at 2θ values of approximately 26°, 38°, and 43°, which are attributed to the existence of graphite, boron carbide, and copper, respectively. Specimen C1 exhibits visible pure copper. The presence of weak reinforcing peaks is attributed to the deficiency in the copper matrix. The C2 peaks of boron carbide(B_4C) and carbon(C) are lower in the hybrid composite sample, indicating both reinforcements. However, it can be observed that the peaks of boron carbide(B_4C) and carbon(C) in C4 exhibit greater significance than those in C2, thereby suggesting that the heights of the peaks grow with an increase in reinforcement content. The obtained samples show strong peaks of copper.

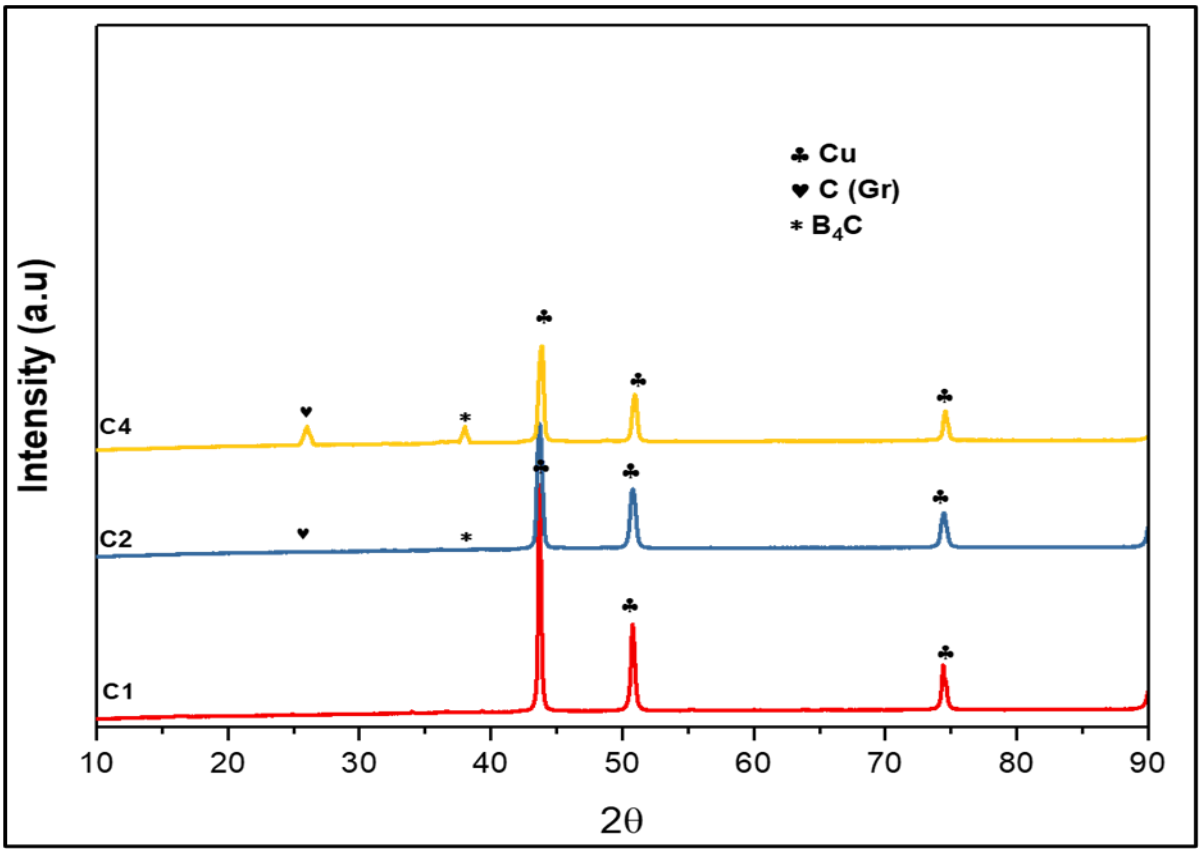

Figure 5.2 XRD pattern of sintered composites.

Based on the X-ray diffraction (XRD) analysis, it can be determined that there is no chemical reaction between copper (Cu) and boron carbide (B_4C). The X-ray diffraction (XRD) data of the hybrid composite specimen C4 exhibit the most elevated peak intensities among all the specimens. The observed phenomenon can be attributed to the efficient dispersion of reinforcement particles throughout the copper matrix. Additionally, the increased content of reinforcement particles is accountable for the heightened peaks.

Figure 5.3 displays the microstructure of (C3) composites captured by high-resolution transmission electron microscopy (HRTEM). The morphology of the (C3) hybrid composite is shown in Figure 5.3(a), where it is evident that the particles of graphite and boron carbide are evenly and densely dispersed throughout the matrix without any obvious agglomerates. The HRTEM image (Figure 5.3(b)) displays the distinctive lattice fringes of boron carbide and graphite. The crystal lattice exhibits edges with a d-spacing of around 0.44 nm, which can be attributed to the (101) plane of rhombohedral B_4C(Bai et al., 2018). Additionally, fringes with a d-spacing of 0.34 nm correspond to the (002) planes of hexagonal carbon.

Figure 5.3(c) provides an enlarged bright field image (a) version. Figure 5.3(d) demonstrates that the EDS spectra confirm the distribution of boron carbide and graphite particles within the copper matrix.

To determine the dispersion of reinforcements within the composite material, (EDS) elemental mapping technique is employed. This technique utilizes a Scanning Electron Microscope (SEM) to analyze the distribution of various elements, such as Copper (Cu), Chromium (Cr), Carbon (C), and Boron (B), within the different sintered specimens. The even distribution of reinforcements significantly affects the tribological characteristics of composite materials. The outcomes depicted in Figure 5.4 illustrate that the (SEM) images, along with the (EDS) element mapping analysis performed on the C1, C2, and C4 specimens, have identified the presence of copper (Cu), chromium (Cr), boron (B), and carbon (C) elements.

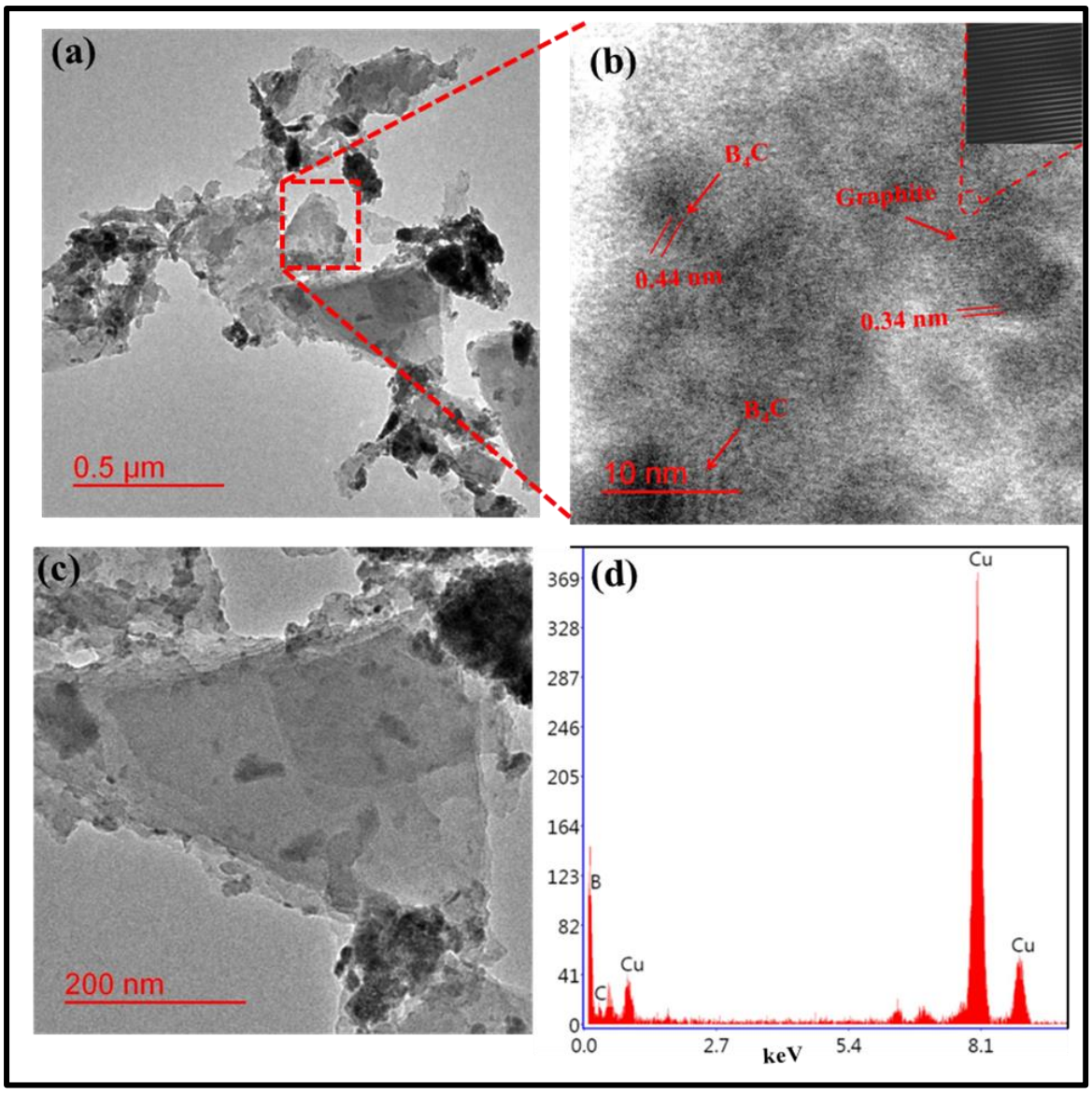

Figure 5.3. (a)The bright field image demonstrates the boron carbide(B_4C) and Gr. Reinforcement within the matrix, (b) HRTEM image of composite with inset IFFT image, (c) enlarged view of bright field image (a), (d) EDS spectrum of C3 composite.

The micrographs indicate the absence of cracks within the composites. The uniform dispersion of the reinforcing particles within the matrix demonstrates the effectiveness of the powder metallurgy method. Pores are rarely visible in the micrographs obtained through scanning electron microscopy. The uniformity and evenness of the dispersion of Graphite and B4C particles were observed in all three formulations, as depicted in Figure 5.4.

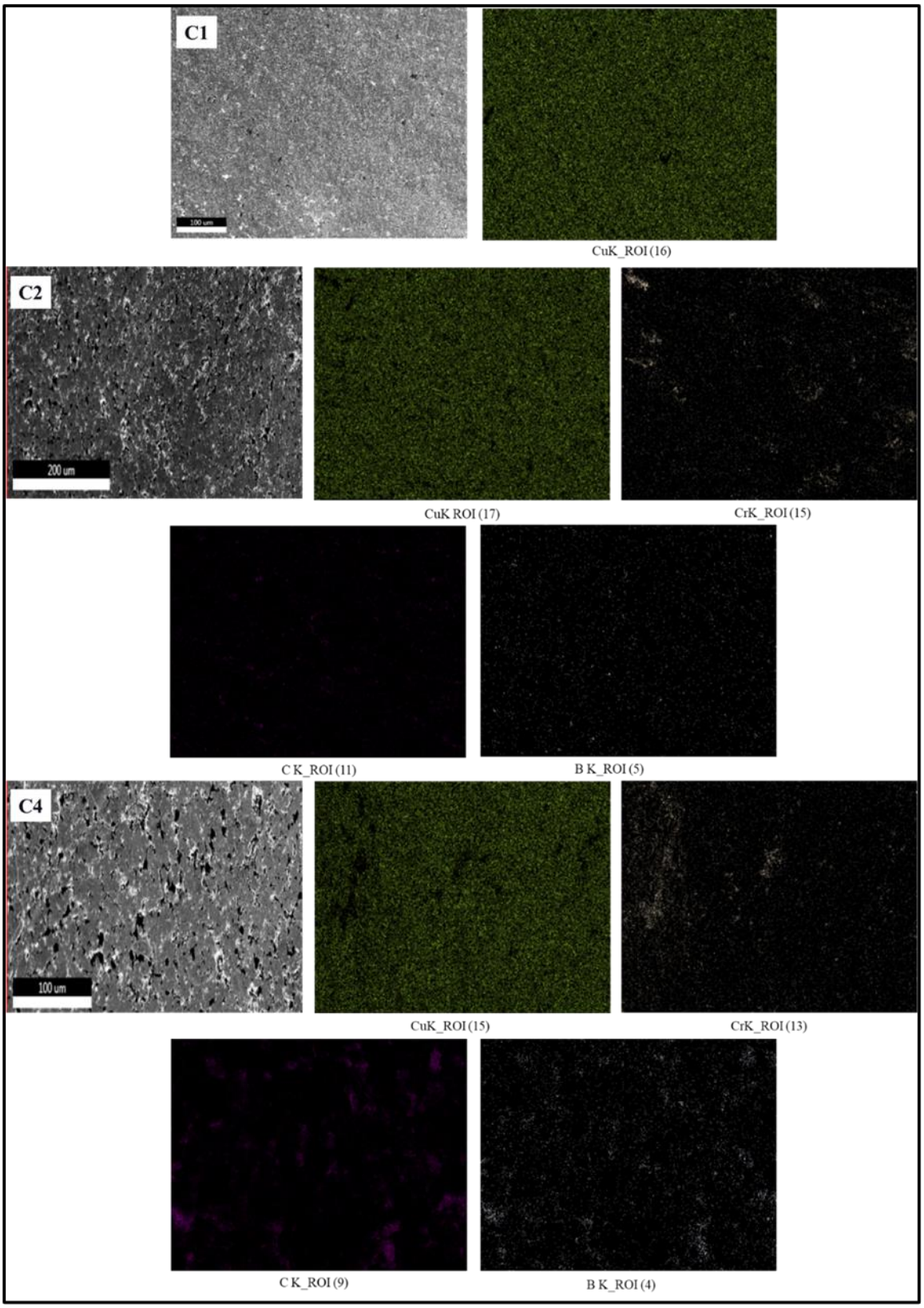

Figure 5.4. Element mapping of elements (Cu, Cr, C, and B) in C1, C2, and C4 specimens.

Even the presence of graphite and B_4C particle aggregations at the highest content, the absence of microcracks indicates that the matrix and particles exhibited satisfactory interfacial strength in the composites. The elemental mapping spots for elements boron(B) and carbon(C) also increased with the higher concentration of boron carbide(B_4C) and graphite (Gr) particles in the composite. This observation is consistent with the findings in Figure 5.4, which further provides evidence of the composite's composition.

5.4 Physical and Mechanical Characteristics

The densities, porosity, hardness, and compressive strength of the sintered specimens are illustrated in Figure 5.5 (a)-(d). The study indicates that the sintered densities of composite specimens are comparatively lower than those of copper specimens that are not reinforced. Upon the introduction of reinforcement particles into the matrix, there is a significant reduction in the density of the resulting composites. The incorporation of a 3% reinforcement results in a reduction of composite density from 8.50 gm/cm^3 to 7.48 gm/cm^3. Moreover, the increase in reinforcement content reduces the density of composites within the matrix. The reduction in thickness of composites is observed with an increase in the proportion of graphite and B_4C due to the lower density of graphite (2.5 g/cm^3) and B_4C (2.5 g/cm^3) particles in comparison to copper (8.96 g/cm^3)(Samal et al., 2013; Wu et al., 2023). The density of a material is subject to the influence of several variables, such as the size, nature, and shape of its constituent particles, as well as its composition. The variety of matrix materials also affects each substance's density. When the proportion of graphite and boron carbide is increased, porosity increases. The copper matrix displays a homogeneous dispersion of graphite and boron carbide particles, although some regions of the matrix tend to form agglomerates, resulting in higher porosity. The agglomeration of B_4C and graphite particles occurs in certain regions, and due to the limited wettability between B_4C and Cu, their interfacial bonding is weak, resulting in the formation of porosity at the interface.

The variation of Vickers hardness number across all sintered specimens is depicted in Figure 5.5 (c). The examination findings revealed that the composites' hardness exhibited significant increases up to a weight percentage of 6 wt.% of Gr-B_4C, after which it experienced a decrease in value-adding 6 wt.% Gr-B_4C reinforcement into the copper matrix significantly enhances hardness, with a recorded value of 97.3HV. This represents an enhancement of 70.1% compared to the hardness value of pure copper, which is 57.2HV. The initial hardness improvement of the composite specimen is attributed to the B_4C and Cr, which have a harder character and more hardness than the Cu matrix. The copper matrix's hardness has increased due to the addition of hard B_4C ceramic particles(Singh and Gautam, 2019). Diamond and cubic boron nitride are the two known materials, with boron carbide coming in third. The improved hardness of the composites is a result of the B_4C particle's ability to inhibit dislocation motion and the uniform dispersion of these reinforcing particles in the Cu matrix during the ball milling process (Baradeswaran et al., 2014; N. Kumar et al., 2023; Prajapati and Chaira, 2019). The observed decrease in hardness of the composite sample, after the addition of 6wt.% reinforcement in the matrix, can be attributed to the presence of graphite. This is due to the relatively softer nature of Graphite, which exhibits lower hardness compared to the Cu matrix. The rise in porosity within the composites leads to the clustering of Gr-B_4C particles in the Cu matrix, resulting in a decline in the hardness of specimens containing a Gr-B_4C concentration exceeding 6 wt.%.

Figure 5.5(d) displays the variations in compressive strength of the prepared specimens.

The compressive strength of specimens with varying B_4C and graphite content exhibited a similar pattern to the hardness of the composites, as depicted in Figure 5.5 (c). Including Graphite content in the matrix leads to a decrease in the compressive strength of the composite specimens. Adding up to 6% wt. of Gr- B_4C reinforcement to composites has been found to increase their compressive strength. It results from the reinforcement particles' uniform

dispersion strengthening in the matrix phase, stabilizing the composite's matrix and stopping it from deforming, providing substantial hardening and strengthening properties. The composite's maximum compressive strength of 517 MPa is reported for (C3), while it decreases to 429 MPa for (C4). Additionally, a decrease in the composites' compressive strength is visible. The composite containing 6% wt. of Gr- B_4C exhibits a low compressive strength value due to an increasing in porosity and non-uniformity of the matrix in some areas with a higher percentage of reinforcing phase. Compared to pure copper, the compressive strength has been reduced due to graphite's inherent self-lubricating properties and softer nature.

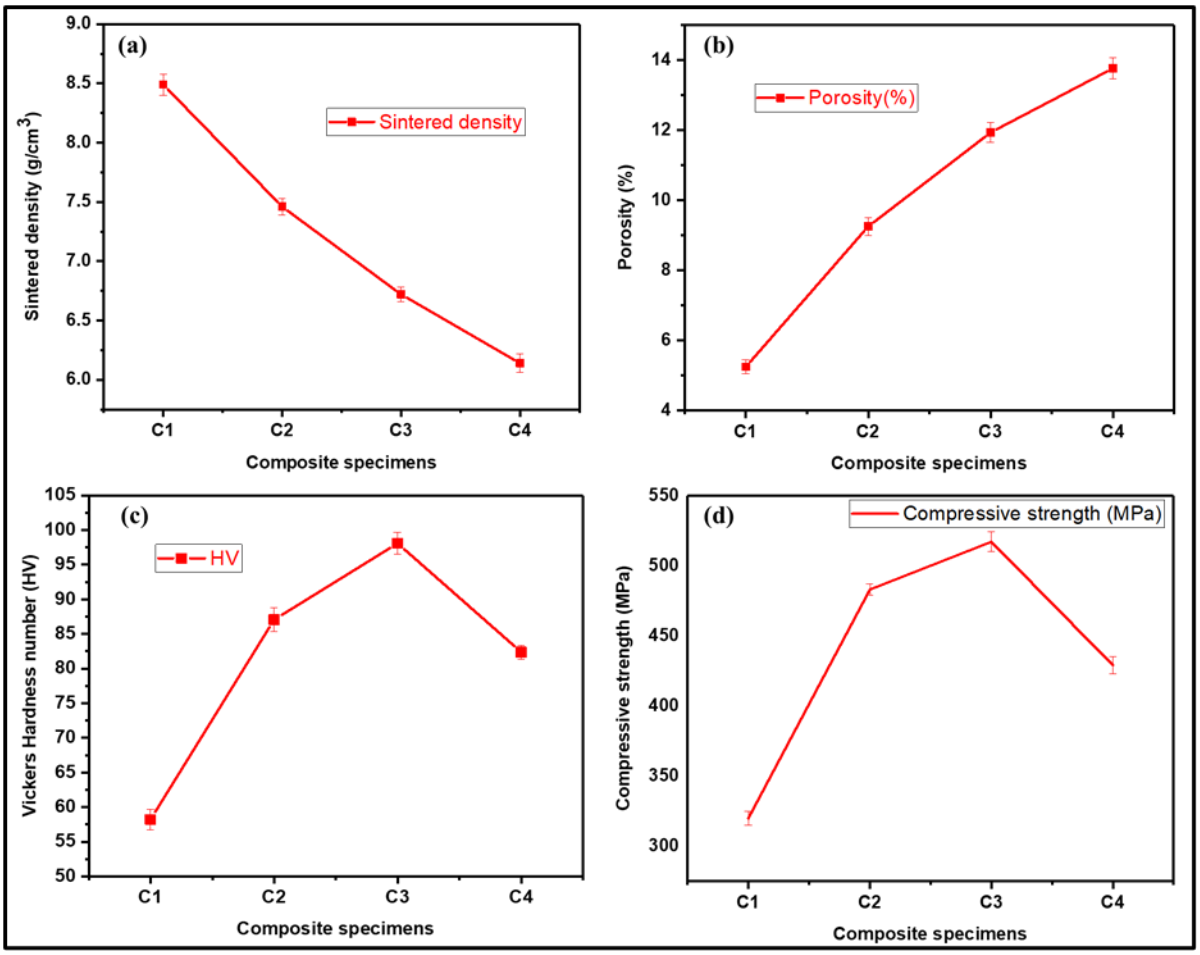

Figure 5.5 The variation in (a)Sintered density, (b) Porosity, (c)Vickers hardness, (d) Compressive strength

5.5 Dry sliding friction and wear of copper-based composites

5.5.1 Effect of reinforcements

The wear rate of specimens with different reinforcement concentrations at a sliding speed of 3 m s−1 is depicted in Figure 5.6 (a). The wear rate decreases upon the addition of graphite and B_4C into the Cu matrix. The wear rate of the C4 specimen exhibits a reduction of 33% and 98% when compared to the wear rates of the C3 and C2 specimens, respectively, for a 40 N load. Additionally, the C4 specimen demonstrates a 124% decrease in wear rate compared to pure Cu. The specimen denoted as C4 exhibited the most significant level of wear resistance among the composites tested. The composite materials' wear resistance enhancement is achieved by establishing an effective interfacial bonding between the matrix phase and reinforcement particles, such as Gr- B_4C. Including B_4C particles with high hardness in the composite material restricts plastic deformation and reduces wear rates. As a result of this particular circumstance, a reduced amount of material is extracted from the pin surface, and there is a decrease in the interaction of composite material with characters that are subject to abrasion. The graphite particles serve as a solid lubricant and generate a lubricating film on the opposing surface, thereby reducing the wear rate. The literature reports comparable results in cases where a soft matrix is followed by hard silicon carbide and graphite particles (Jamwal et al., 2020). The variations in the COF value of the reinforcements are depicted in Figure 5.6 (b). The COF values for specimens C1, C2, C3, and C4 are 0.772, 0.619, 0.578, and 0.512 when subjected to a 40 N load. The COF for the C4 specimen exhibited a reduction of 13% and 21% compared to the C3 and C2 specimens, respectively. Moreover, the COF value for the C4 specimen was 51% lower than that of the C1 specimen. The study demonstrated that an increase in the reinforcement ratio decreased the coefficient of friction. The dispersion of graphite particles results in forming an intermediate layer, thereby reducing the direct contact of the composite pins with the counter surface. The composite’s low friction results from the passivation of the

deteriorated surfaces by the combined action of B_4C and graphite, which forms tribo-layer films (Essa et al., 2017). The observed phenomenon can be attributed to the favourable solid lubricant properties of graphite and the rapid formation of boron oxide (B_2O_3) layer by B_4C, which played a crucial role in reducing the coefficient of friction (Çelik and Seçilmiş, 2017). The existing literature indicates that a similar result is observed when a soft matrix contains both rigid titanium carbide and graphite particles (V. Kumar et al., 2023; Rajkumar and Aravindan, 2011).

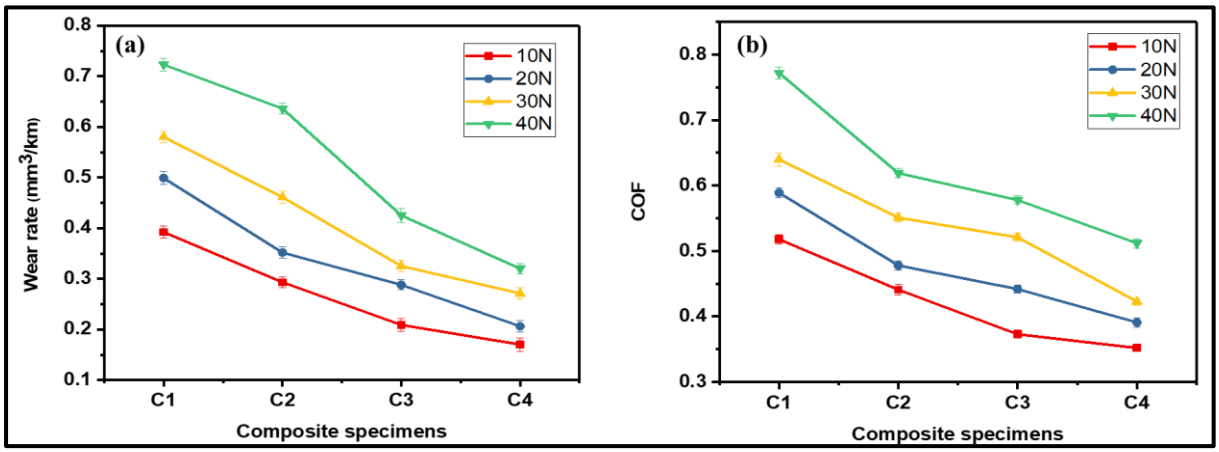

Figure 5.6 Influence of reinforcement on (a) wear rate (b) COF at a sliding velocity of 3 m/s

5.5.2 Effect of applied load

The wear rates of pure Copper C1 and composite materials C2, C3, and C4 specimens under different loads (10 N–40 N) at a sliding speed of 3 m/s are depicted in Figure 5.7 (a). Studies indicate that lower loads correspond to a comparatively lower rate of wear, whereas higher loads result in an escalation of wear exhibited by the specimen. In wear testing, the actual contact area is consistently smaller than the apparent contact area due to the textured nature of the specimen's surface. As the applied load increases, the effective contact area between the surfaces also increases, increasing the plastic deformation of the asperities. This phenomenon ultimately leads to a higher rate of wear of the specimens. The wear rate of pure copper exhibited a consistent increase, which can be attributed to the deformation of its microstructure

and the gradual formation of a thin oxide layer on the contact surface. At lower loads, the formation of an oxide film acts as a barrier to prevent direct contact between copper and the counter face. Following increased applied load, the soft copper material observed a significant degree of plastic deformation. The degradation of the oxidative layer due to continuous sliding may result in the emergence of a third body between the surfaces, thereby increasing the wear rate of composite materials. Earlier research literature also reports similar findings(Ankit et al., 2023).

Figure 5.7 (b) illustrates the fluctuation in COF about the applied load for specimens of pure Copper C1 and composite materials C2, C3, and C4 under varying loads (ranging from 10 N to 40 N) at a sliding speed of 3 m/s. It has been observed that the coefficient of friction increases along with the usual weight. Under all load circumstances, the pure copper specimen has a higher coefficient of friction. the adhesive properties of tribo contact cause the soft copper matrix to migrate to a harder countertop surface. As the applied load increases, more plastic deformation occurs, increasing the coefficient of friction value. However, in all composites, it is also possible for the B_4C particles to emerge from the pin surface under high stress and contribute to a rise in the coefficient of friction value.

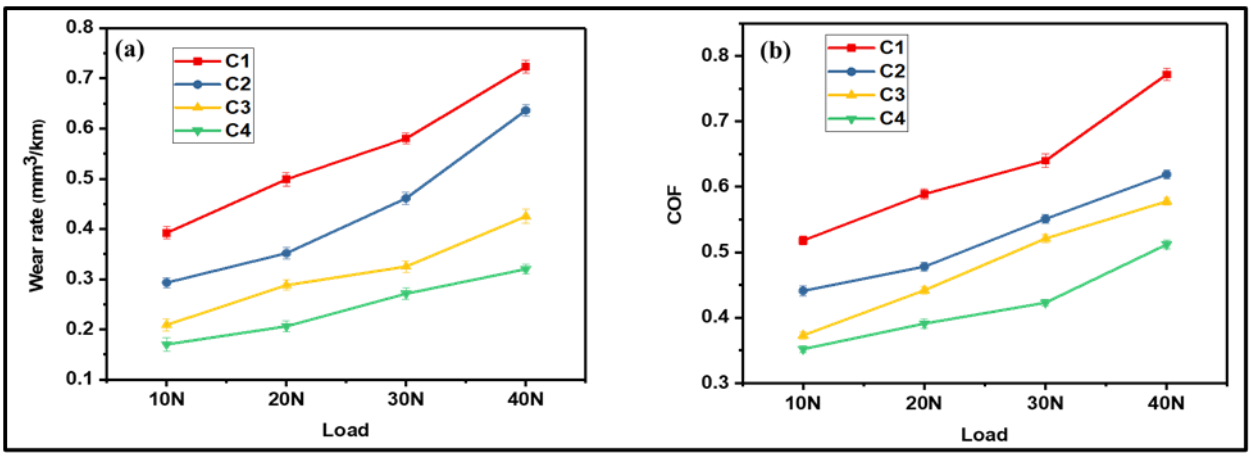

Figure 5.7 Influence of load on (a) wear rate and (b) COF at a sliding velocity of 3 m/s

5.5.3 Effect of sliding speed

The wear rate for each specimen is shown in Figure 5.8 (a), with a load of 40 N and sliding speeds of 1 m/s, 2 m/s, and 3 m/s. The results indicate that the wear rate of the pure copper specimen C1 is comparatively higher than that of the composites with a higher weight percentage of reinforcements, which exhibit lower wear rates at a sliding speed of 1 m/s. The average wear rate of each composite is higher when sliding at a velocity of 3 m/s than when sliding at a velocity of 1 m/s. The present investigation reveals that the sliding speed has a minor impact on the wear rate of the hybrid composites being examined. The frictional force increases as sliding speed increases from 1 m/s to 3 m/s, which causes additional reinforcing particles to be drawn out of the composite. Pull-out particles are momentarily trapped between the contact surfaces. The wear rate can be accelerated by hard ceramic particles in composites breaking off the surface and acting as a third body at the contact (Siddesh Kumar et al., 2020). The COF values at 40 N normal load and sliding velocities of 1 m/s, 2 m/s, and 3 m/s are depicted in Figure 5.8 (b), illustrating their fluctuation. The present study has revealed that the COF of the hybrid composites exhibits an increase in response to variations in sliding speed. The B_4C ceramic particles underwent mechanical comminution between the contacting surfaces, forming an adherent film due to the spread of graphite particles at the contact surface. The adhering films formed at the contact surface exhibit reduced effectiveness over shorter durations due to the higher sliding speed. Upon reaching a specific sliding distance, the film detaches from the contact surface and is expelled from the contact area. The high sliding speed facilitates contact between the counter surface and the recently formed composite surface, increasing the coefficient of friction.

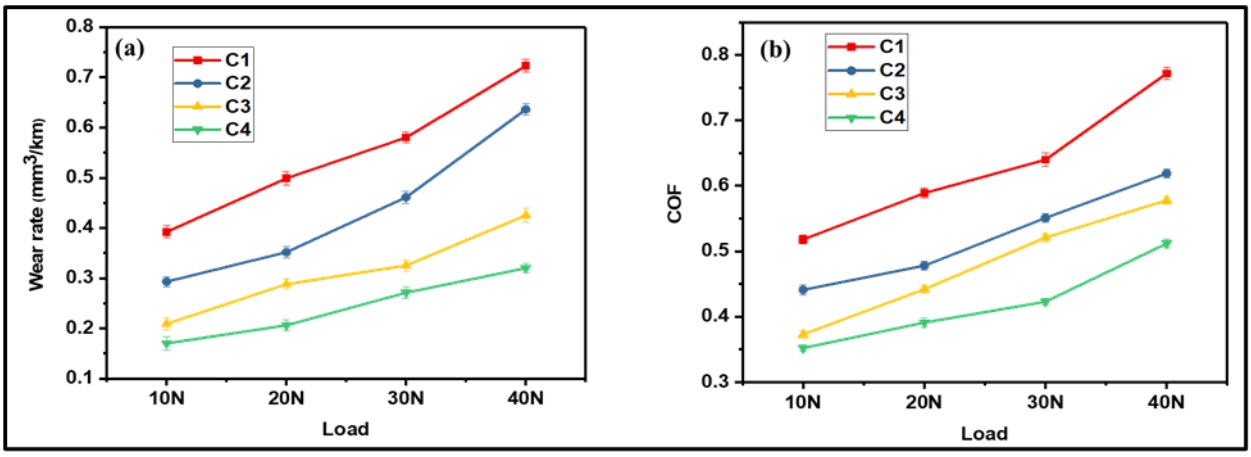

Figure 5.8 Influence of load on (a) wear rate and (b) COF at a sliding velocity of 3 m/s

5.6 Analysis of deteriorated surface

5.6.1 deteriorated surface at a normal load of 40 N for C1&C2 specimen

A comprehensive analysis of the microstructural features of deteriorated surfaces of pure copper and its hybrid composites was conducted using scanning electron microscopy (SEM). The SEM images in Figure 5.9 exhibit the deteriorated surfaces of the C1 and C2 specimens at varying sliding speeds (1, 2, and 3 m/s) while subjected to an identical load of 40 N. The findings presented in Figure 5.9(a) indicate that the surface of the pure copper specimen C1 experienced delamination along with an oxide layer at a lower sliding velocity of 1m/s. However, Figure 5.9(c) illustrates a severe delamination at a higher sliding speed of 3 m/s. The experiment involved subjecting a pure copper specimen to rubbing with a hardened EN30 steel disc, resulting in substantial substance loss.

This was attributed to the sharp asperities of the steel counterpart, which deeply cut into the surface of the pure copper. Consequently, the coefficient of friction (COF) and wear rate of the pure copper specimens were increased. Severe delamination was observed on the deteriorated surfaces. The illustration in Figure 5.9 (e) demonstrates the existence of significant delamination on the deteriorated surface. Smooth grooves on the surface are observed at low velocities. Upon increasing the velocity, a substantial occurrence of delamination has been observed.

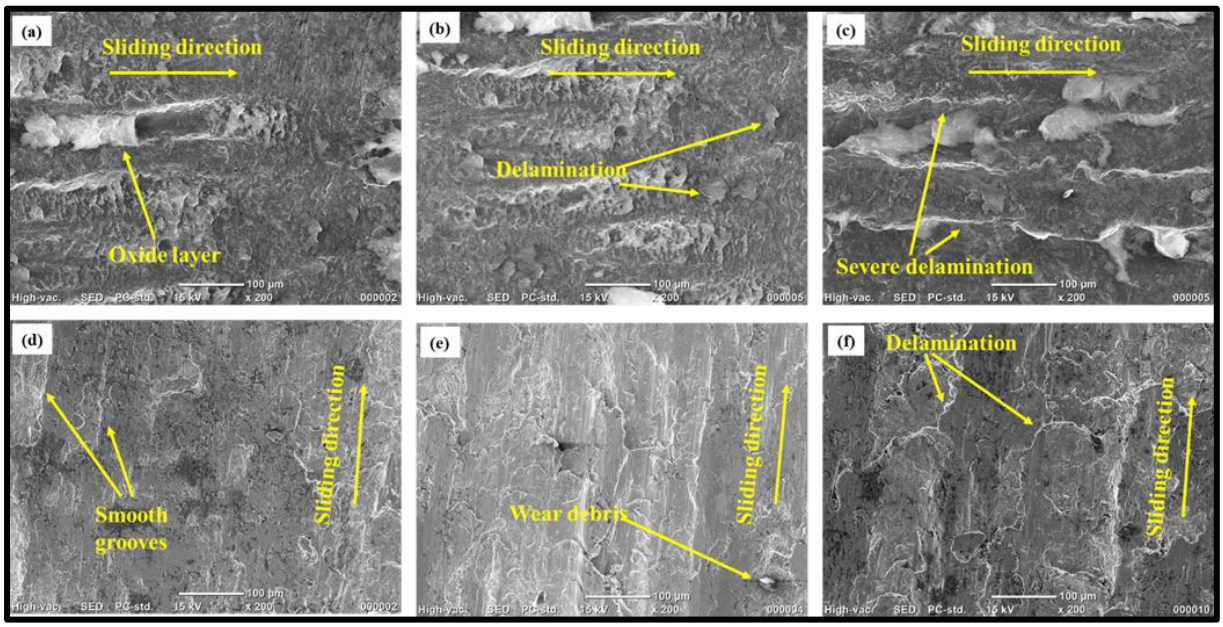

Figure 5.9 (SEM) images of the deteriorated surface at 40 N load for (a) C1 specimen at 1 m/s, (b) C1 at 2 m/s, (c) C1 at 3 m/s, and (d) C2 at 1 m/s (e) C2 at 2 m/s (f) C2 at 3 m/s velocity.

5.6.2 deteriorated surface at a normal load of 40 N for C3&C4 specimen

The deteriorated surfaces in the composites C3 and C4 are more or less the same as they are at low sliding velocities (Figures 5.10 (a) and (d)). Still, they change more morphologically at high sliding velocities (Figures 5.10 (c) and (f) as the amount of B_4C and graphite particles increases. The surface of the C3 specimen exhibits smooth ploughing, delamination, and delamination cracking. On the other hand, the C4 specimen displays a smooth plough mark and abrasion mark with an oxide layer. The wear behavior of this composite predominantly involves adhesion, leading to delamination, primarily due to strong friction force between the ductile matrix and mating surfaces. However, introducing graphite (Gr) as reinforcement disrupts this mechanism by acting as a lubricating layer, mitigating adhesion and preventing delamination. Graphite's self-lubricating properties create a protective barrier, minimizing friction and enhancing wear resistance. Initially, copper undergoes abrasion due to wear between the copper matrix and the metallic counter surface. Subsequent exposure of fresh B_4C

hard particles serves as wear-resistant agents, alongside the formation of B_2O_3 oxide, which acts as a protective layer, effectively reducing wear. This dual action of B_4C contributes to both abrasion resistance and forming a protective layer, which is crucial for the composite's tribological performance. Increased B_4C and graphite content shifts the wear mechanism from delamination to a combination of abrasive, oxidative, and delamination wear, diversifying the material's overall tribological behavior.

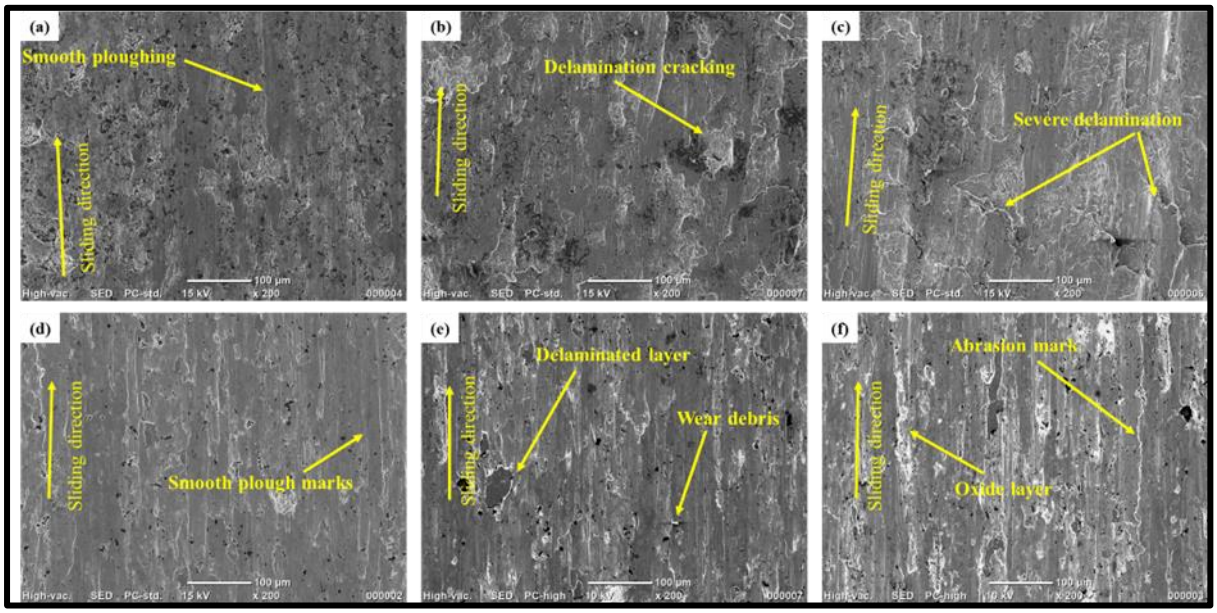

Figure 5.10 (SEM) images of the deteriorated surface at 40 N load for (a) C3 specimen at 1 m/s, (b) C3 at 2 m/s, (c) C3 at 3 m/s, and (d) C4 at 1 m/s, (e) C4 at 2 m/s (f) C4 at 3 m/s velocity.

5.6.3 EDS spectrum of the deteriorated surface at 40 N load

Figure 5.11 displays the EDAX results for the worn surface of C2 and C4 specimens subjected to a load of 40 N and a sliding speed of 3 m/s. The EDS spectrographs of the C2 and C4 specimens are depicted in Figure 5.11 (a) and (b), respectively. The spectral analysis verifies the existence of copper as the most predominant element, succeeded by chromium (Cr), boron (B), iron (Fe), oxygen (O), and carbon (C) in the form of graphite.

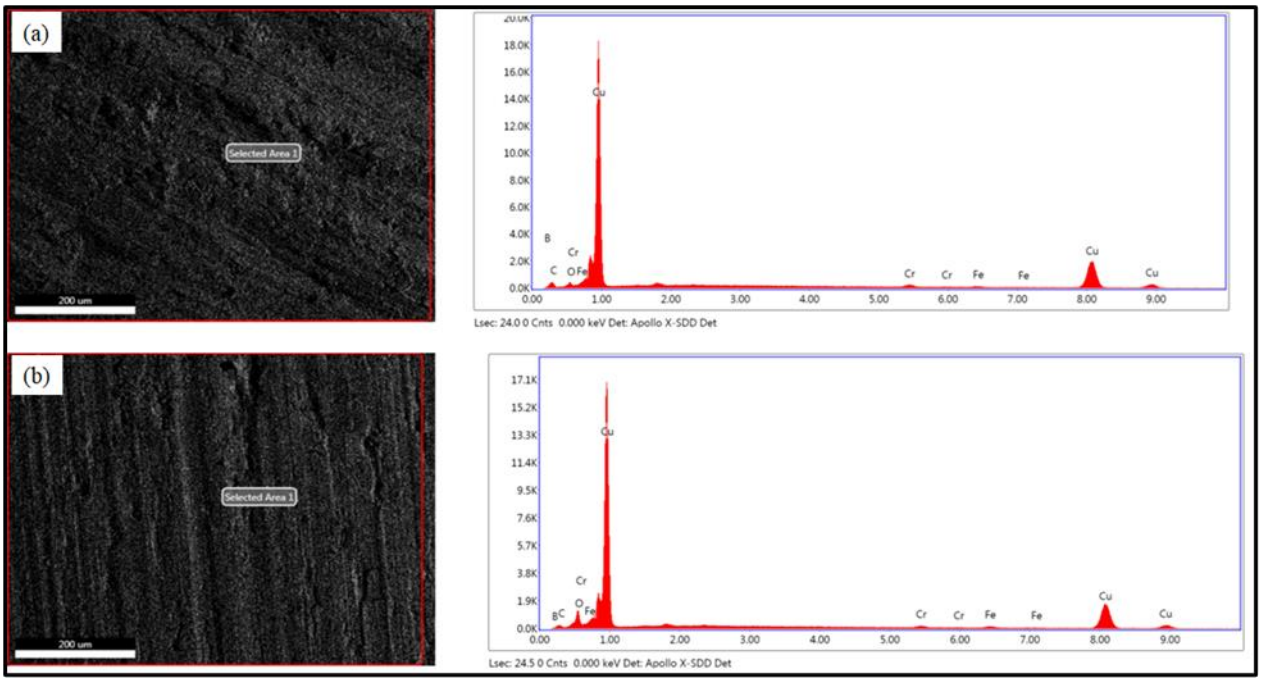

Figure 5.11. (EDS) of the deteriorated surface at 40 N load (a) C2 specimen at 3 m/s, (b) C4 at 3 m/s velocity.

5.6.4 Atomic force microscopy (AFM) analysis of deteriorated surfaces

The deteriorated surfaces of the C1, C2, C3, and C4 specimens were also analyzed using AFM. The three-dimensional profile of the visualization of deteriorated surfaces can also be observed using atomic force microscopy (AFM), as depicted in Figure 5.12. The utilization of (AFM) is highly appropriate for quantifying surface roughness and visualization of surface micro-texture in deteriorated composite specimens. When assessing the surface topography of composites, a dimension of 50 µm is considered. All depicted specimens exhibited a surface texture that correlated to waviness. The observation reveals that the C1 specimen, made up purely of copper, shows a significantly larger peak-to-valley range of -2 µm to 3 µm compared to the other composite specimens. This indicates that there is more wear in the pure copper specimen. The pattern that can be seen in the maximum peak-to-valley range decreases as the content of the Gr and B_4C particles is increased from C2 to C4 in the specimens depicted in Figures 5.12 (b) to (e). The specimen designated as C4 exhibited the smallest range between its peak and valley measurements. The primary factor contributing to the decrease in surface roughness in

the composite specimen is the wear debris's high hardness and its inability to adhere to the rubbing surfaces. This results in smooth rolling or sliding on the frictional surfaces. Therefore, the hybrid composite specimens demonstrated high effectiveness in preventing wear, as illustrated in Figure 5.12 (Ali and Xianjun, 2019). This occurred when a load of 40N was applied, and the sliding velocity was set at 1m/s. The values recorded for this specimen ranged from -800 nm to +800 nm. These results support the wear results, showing that the C4 specimen exhibits the least wear.

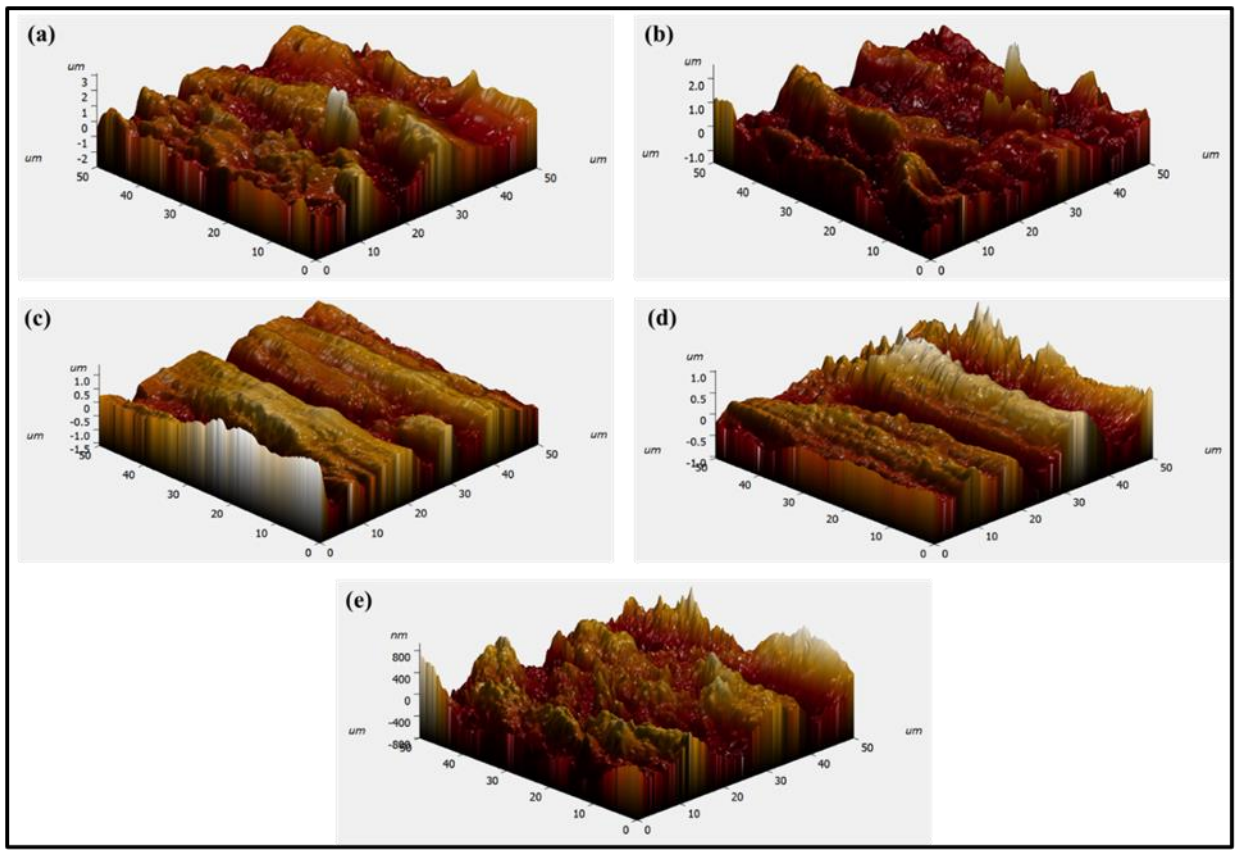

Figure 5.12. Atomic force microscopy (AFM) 3D images of deteriorated surfaces at 40N Load & 3m/s sliding velocity for specimens of (a) C1, (b) C2, (c) C3, (d) C4 and (e) C4 specimen at (40N &1m/s).

5.6.5 Topographical parameters of worn surface

Additionally, Figure 5.13 presents the 2D line graphs of the AFM photographs, which allow for the examination of the frequency and range of peaks and valleys in each photograph. The x-axis represents the peak and valley values range, while the y-axis indicates the total count. The increase in the content of Gr and B_4C, as shown in Figure 5.13(b) to (e), leads to a reduction in the value of peaks and valleys, indicating a less rough surface profile. The surface topographical criteria were computed for the various Atomic force microscopy (AFM) shots of the specimens, and their corresponding values are presented in Table 5.1. The tribological characteristics of deteriorated specimens are assessed by analysing texture data from surface scans, which provide measurements of specific criteria that significantly influence these characteristics (Raoufi et al., 2007). The topographical criteria consist of various measurements, such as the average surface roughness (Sa), root means square roughness (Sq), area peak to valley height (St), skewness of the plane (Ssk), and kurtosis of the plane (Sku)[51]. The Sa value is determined using atomic force microscopy (AFM). It represents the average height measurement taken across the entire surface area and is frequently employed to assess the roughness of deteriorated surfaces. This supports the identification of variations in the overall profile height order and serves as a means of monitoring the validity of the fabrication method utilized. St, determined by the vertical distance between the top and bottom points in the defined region, measures the overall roughness of the specimen's surface. Sq is the surface height spread used to calculate the criteria for skew and kurtosis. Sq is expected to provide more accurate roughness estimates for noticeable variations from the mean plane than average roughness. It is considered that the Skewness (Ssk) value, which measures the uniform divergence of the deteriorated surface from the mean plane, is more susceptible to abruptly high peaks or deep valleys. Ssk describes the capacity for bearing loads. An improved bearing surface is considered to have a negative skew value. The distribution of spikes below and above

the average plane is determined for deteriorated surfaces using the Kurtosis (Sku) value, and this evaluation is mainly utilized to regulate stress fractures. If the kurtosis value of a surface is more than three (>3), we describe it as spikey, but if it is below three (3), we describe it as bumpy. Kurtosis value of precisely three (3) states of random surfaces (Kumar and Rao, 2012).

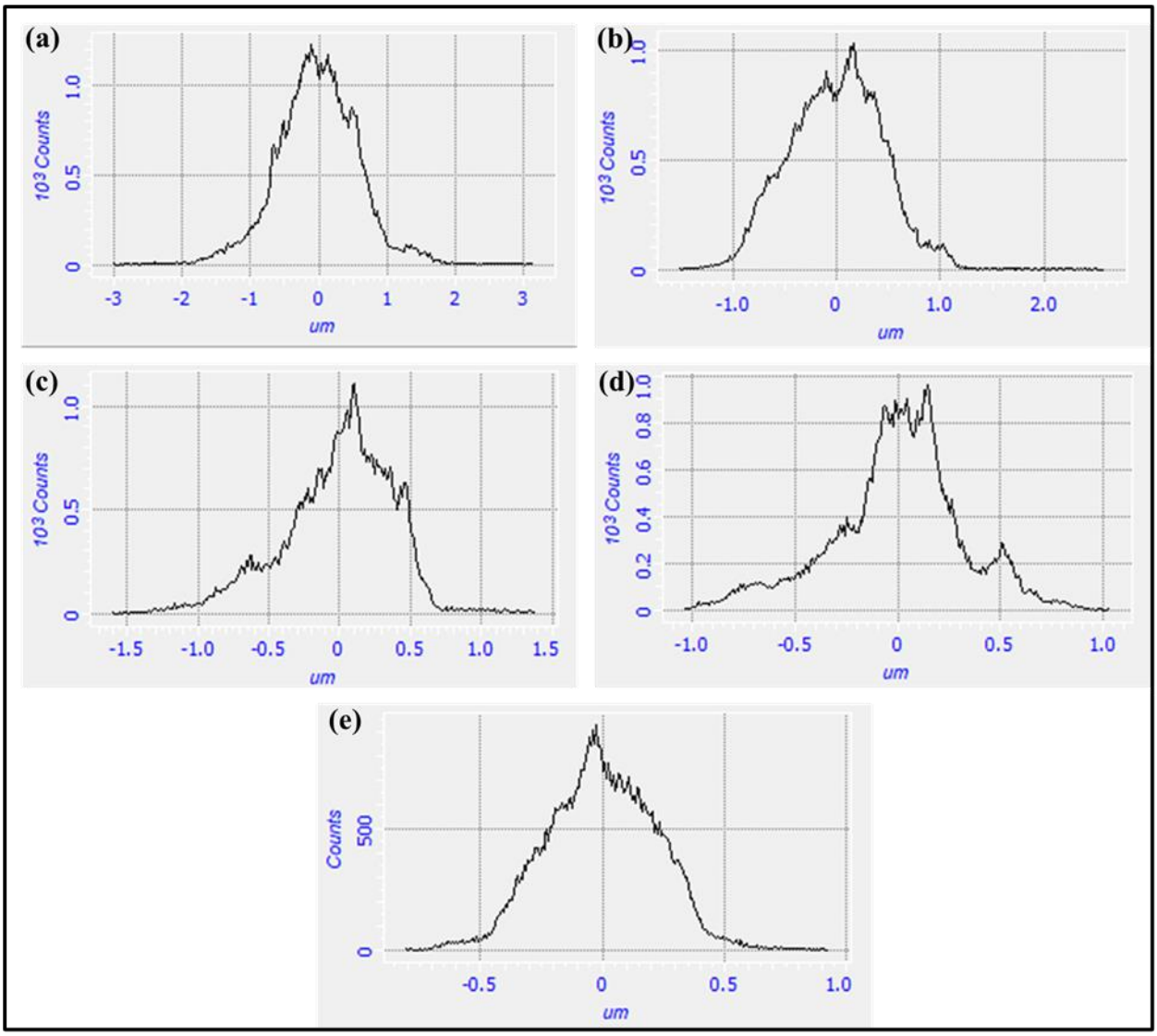

Figure 5.13 AFM 2D surface profile examination of deteriorated surfaces at 40N Load & 3m/s sliding velocity for specimens of (a) C1, (b) C2, (c) C3, (d) C4 and (e) C4 specimen (40N &1m/s).

Table 5.1. Topographical parameters of all specimens at 40N load and 3m/s velocity.

Composite specimen	Average roughness S_a (µm)	Root mean square roughness S_q (µm)	Area peak-to-valley height S_t (µm)	Skewness S_{sk}	Kurtosis S_{ku}
C1	0.457	0.597	6.147	0.062	4.596
C2	0.360	0.445	4.103	0.044	3.615
C3	0.298	0.383	2.986	-0.389	3.475
C4	0.238	0.316	2.072	-0.508	3.168
C4 (1 m/s)	0.183	0.232	1.658	-0.794	3.058

According to Table 5.1, under a load of 40N and a sliding velocity of 3m/s, the average roughness Sa value decreases from 0.457 µm to 0.238 µm as the reinforcement content increases. We also found a decrease in Sa value up to 0.183 µm for the C4 specimen by reducing sliding velocity from 3 m/s to 1 m/s. For each sample, the Sa values are lower than the Sq value of that sample. The St value also continues to reduce from the C1 specimen to the C4 specimen similarly. Table 5.1 further shows that negative skewness values indicate that deep valleys predominate in the chosen region, whereas positive skewness values indicate that peaks are predominate. Consistent negative skewness values indicate the presence of cracks or indications of valleys. Negative values for Ssk indicate a significant ability to bear loads. As Gr and B_4C content rises, the skewness value becomes more negative, further showing an increase in load-bearing capacity. This capacity peaks at 4.5 wt% of each Gr and B_4C particle (Ssk for C4 specimen is 0.508). For composites (C2 to C4 specimen), the kurtosis value Sku is near 3, indicating that there are comparatively fewer high peaks and deep valleys throughout the examined region and that the surface is bumpy. Although Sku value for the pure copper C1

specimen is 4.596, which is significantly greater than 3, its spread will be characterized by many high peaks and deep valleys with surface spikes. The C1 specimen has more surface roughness than other specimens due to its high Sku and St values. Peak heights and valley depths are highly associated with Sku, which may account for the relationship.

5.7 Conclusion

The The Graphite (Gr) – boron carbide(B_4C) reinforced copper matrix composite materials were successfully produced by implementing the powder metallurgy technique. The investigation has been carried out to determine the effect of reinforcements on the tribological behavior of composite materials. The following conclusions can be made based on the results and the discussion:

1) The SEM, HRTEM and EDS facilitated the examination of microstructure, revealing a nearly homogeneous dispersion of particulate matter and verifying the existence of graphite and B_4C particles. The densities of hybrid materials were observed to decrease upon introducing reinforcement materials such as Gr and B_4C, which possess lower densities than the base material. The cluster formation leads to a reduction in effective heating as the amount of reinforcement rises. The decrease in the thermal capacity of the composite material results in a corresponding rise in porosity.
2) The composites' hardness and compressive strength increased appreciably to a Gr- B_4C of 6 wt.% before declining. The hardness can increase to 97.3 HV with the inclusion of 6 wt.% Gr- B_4C reinforcement is a 70.1% increase over base material (57.2 HV). The C3 specimen exhibits the highest compressive strength. Additionally, the composites' compressive strength decreased due to the graphite's softness and the brittle character of the B_4C particles.
3) It has been found that as the reinforcing percentage rises, the wear rate and COF of composites decrease. When the reinforcing component reaches 9%, the wear rate is at

its lowest due to the collaborative impact of both graphite (Gr) and B_4C particles. This synergistic effect between Gr and B_4C significantly contributes to the minimized wear observed in this particular specimen.

4) Delamination is the leading cause of wear for pure copper specimens, according to analysis of the worn surface. The introduction of graphite mitigates delamination through self-lubrication properties, while B_4C particles exhibit dual functionality by resisting wear and contributing to forming a protective layer alongside B_2O_3 oxide. Increased proportions of both B_4C and graphite prompt a transition in the wear mechanism of the composite from predominantly delamination to a combined action involving abrasion, oxidation, and delamination wear.
5) The composite specimen exhibited improved loadbearing capacity and reduced roughness values when reinforced with 4.5 wt.% each of B_4C and Gr, as indicated by the topographical parameters.